Published online 3 July 2010 *Nucleic Acids Research, 2010, Vol. 38, No. 20* ***7089–7099***
doi:10.1093/nar/gkq597

Magnetic tweezers measurements of the nanomechanical properties of DNA in the presence of drugs

Domenico Salerno[1,*], Doriano Brogioli[1], Valeria Cassina[1], Diana Turchi[1], Giovanni Luca Beretta[2], Davide Seruggia[1], Roberto Ziano[1], Franco Zunino[2] and Francesco Mantegazza[1]

[1]Dipartimento di Medicina Sperimentale, Universita' di Milano - Bicocca, via Cadore 48, Monza (MI) 20052 and [2]Dipartimento di Oncologia Sperimentale e Medicina Molecolare, Fondazione IRCCS Istituto Nazionale Tumori, via Venezian 1, Milano (MI) 20133, Italy

Received April 12, 2010; Revised June 16, 2010; Accepted June 17, 2010

ABSTRACT

Herein, we study the nanomechanical characteristics of single DNA molecules in the presence of DNA binders, including intercalating agents (ethidium bromide and doxorubicin), a minor groove binder (netropsin) and a typical alkylating damaging agent (cisplatin). We have used magnetic tweezers manipulation techniques, which allow us to measure the contour and persistence lengths together with the bending and torsional properties of DNA. For each drug, the specific variations of the nanomechanical properties induced in the DNA have been compared. We observed that the presence of drugs causes a specific variation in the DNA extension, a shift in the natural twist and a modification of bending dependence on the imposed twist. By introducing a naive model, we have justified an anomalous correlation of torsion data observed in the presence of intercalators. Finally, a data analysis criterion for discriminating between different molecular interactions among DNA and drugs has been suggested.

INTRODUCTION

Newly conceived anti-cancer drugs are usually scrutinized by considering their biological effects on mesoscopic samples *in vivo* or *in vitro*. Recently, new single molecule tools have been developed in order to test drug activity at the molecular level. Indeed, single molecule techniques have opened new ways for studying biologically and biomedically relevant problems because they are not limited to measuring only ensemble properties (1). Among single molecule techniques, the magnetic tweezers (MTs) technique is well suited to experiments on single DNA molecules (2,3). The MT technique allows us to manipulate small bodies or single macromolecules by connecting them to a micron-sized superparamagnetic bead that, in turn, can be manipulated by means of macroscopic magnetic fields generated by permanent magnets or electromagnets (4). The DNA acts as a tether between the bead and a fixed position, which, in our case, is the inner surface of a capillary tube. Possible manipulations include stretching and torsion of the molecule. Simultaneous measurements of the bead position, applied force and imposed torsion give information about the nanomechanical properties of DNA, including bending and torsional properties (2,5).

Compared to other single molecule tools such as optical tweezers (OTs) (6–11), micropipettes (12) and atomic force microscopy (AFM) (3,13–15), the MTs method is much simpler to implement. Furthermore, the ability to measure torsional properties is a natural feature of MT. Incidentally, this ability has also recently been obtained with OT using unconventional nanoparticles and relative analysis (16,17).

The first pioneering MT studies addressed the topology of individual DNA molecules by measuring DNA extension as a function of the applied force and imposed torsion (18–20). In particular, it has been observed that torsion can produce plectonemes, which influence DNA extension (21). In some high-force or torsional stress conditions, nanomanipulation can also induce denaturation. Due to the chirality of DNA, this is obtained more easily with counterclockwise torsion than with clockwise torsion (2). Subsequently, MTs have been used in other configurations

*To whom correspondence should be addressed. Tel: +39 02 6448 8215; Fax: +39 02 6448 8068; Email: domenico.salerno@unimib.it
Correspondence may also be addressed to Francesco Mantegazza. Tel: +39 02 6448 8209; Fax: +39 02 6448 8068; Email: francesco.mantegazza@unimib.it

and in investigations of DNA in the presence of proteins, enzymes, ligands and drugs. For example, the activity of the gyrase enzyme has been studied by MT and has been demonstrated to exhibit three distinct modes of activity depending on the applied nanomechanical stress (22). Eukaryotic topoisomerase IB has been analyzed with MT by measuring the relaxation time of supercoiled DNA. In the presence of a topoisomerase, it has been shown that it is possible to evaluate the rotational friction of a DNA molecule around the single strand generated by the enzyme (23). On the basis of this work, the MT technique was then used to quantitatively measure the pharmaceutical efficacy of a well-known anti-cancer drug, camptothecin, which inhibits topoisomerase I activity (24). Another enzyme, an RNA polymerase, has been studied by MT techniques; it was revealed that the initiation of the transcriptional process depends on the topology of the DNA (25,26). The effect of a specific anti-cancer drug, cisplatin, has been scrutinized by measuring force versus extension data obtained with MT techniques, and the obtained results have revealed the existence of two separate persistence lengths in kinked DNA in the presence of the drug (27).

Other similar reviews (28–30) have shown that MT techniques can provide an elegant description of single molecule aspects of DNA-ligand binding, which suggests that the use of MT could become a common technique for measuring a ligand's effects on DNA.

We aim to use MT in order to compare the nanomechanical effects induced on DNA in the presence of four different ligands: ethidium bromide (ETBR), doxorubicin (DOXO), cisplatin (CIS) and netropsin (NETRO).

- ETBR is a DNA-intercalating molecule lacking antitumor activity that is used as a laboratory tool for DNA staining (31). It has been reported that ETBR modifies the DNA contour length (32–35) and induces unwinding (36,37).
- DOXO is a well-known DNA intercalating agent, and DNA is recognized as the primary target for its pharmacological action. Despite the central role of DNA binding in the antitumor activity of anthracyclines, available evidence indicates that the inhibition of a specific DNA function is responsible for their therapeutic effects. Indeed, the primary mechanism of cytotoxic and antitumor activity by DOXO is now ascribed to its interference with the function of topoisomerase II. DOXO functions as an enzyme poison by forming a DNA–drug–enzyme ternary complex, which thus stabilizes the cleavable complex in which DNA strands are broken and enzyme subunits are covalently linked to the DNA. Stabilization of the cleavable complex causes specific lethal DNA lesions (i.e. double-strand protein-associated DNA breaks) after collision with enzymes involved in DNA metabolism (38).
- CIS is an antitumor alkylating drug. CIS is a DNA-damaging agent that forms bifunctional adducts. The resultant cross-linked/damaged DNA causes cells to undergo apoptosis (39,40).
- NETRO is a minor groove binder that exhibits antiviral activity by inhibiting the replication of DNA and RNA viruses in mammalian cells (41). NETRO causes overtwisting of the DNA chain, as shown in (42–45).

In the following, we show the results of two different kinds of experiments. First, we measured the dependence of DNA extension on the applied force in the presence of these drugs. Then, we studied the effects of torsion. Both experiments were compared with control data obtained using bare DNA. The results were interpreted according to the available knowledge in the field, and we have experimental results that show new features that are reported here for the first time. Namely, in the case of intercalators, we observed an anomalous dependence in the extension versus twist data, which has been interpreted by introducing an extended naive mechanical model of DNA. Furthermore, we have extracted the dependence of the DNA bending characteristics as a function of twist, and we observed the unique behavior of different drugs. We suggest that these results may form the basis of a quantitative screening for anti-cancer drugs based on single molecule properties.

MATERIALS AND METHODS

Drug characterization

In this study, we used four different DNA binders: DOXO, ETBR (Sigma Aldrich), CIS (Bristol-Myers Squibb) and NETRO (Sigma Aldrich). All binders were diluted in 0.22 μm-filtered de-ionized pure water. For all of the MT measurements we used a fixed drug concentration (5 μM). This concentration is not enough to saturate all the binding sites, but it is sufficient to produce an observable effect on DNA nanomechanics characteristics.

DNA preparation

In the MT experiments, we used a 6964 bp DNA molecule suitably functionalized in order to provide a connection to a mobile support (the magnetic bead) at one end and to an immobile support (the capillary tube) at the other end. It is important to note that the DNA is attached via multiple bonds to both of the supports, which means that the molecule is torsionally constrained and that the magnetic rotation of the bead induces a real torque on the DNA because it cannot swivel around the bonds (2).

To prepare this construct, the DNA tails were functionalized at one end with biotin, for linking to an avidin-coated magnetic microparticle, and at the other end with digoxigenin, for linking to an anti-digoxigenin-coated capillary. The central portion of the DNA consists of a 5780 bp pCMV6-neo plasmid (Origene), while the ends are 537 and 647 bp stretches of the pBR322 plasmid (Stratagene) obtained using a PCR reaction with biotin or digoxigenin-labeled nucleotides, respectively. PCR reactions were performed using two oligonucleotides annealed to the pBR322 plasmid and carrying the restriction enzyme sites NotI (5′-CATATGGCGGCCGC ATGCGCGCATCTCCTTGCATGCACCATTCCTTG

CG-3′) and SacII (5′-CATATGCCGCGGATGGCGCCA TGCGGCCGCATCTCCTTGCATGCACCATTCCTT GCG-3′), respectively, in the presence of two different reverse primers (5′-CTGTCCCTGATGGTCGTCATCT AC-3′; 5′-ATCCATGCCAACCCGTTCCATGTG-3′). PCR was performed in the presence of biotin-16-dUTP or digoxigenin-11-dUTP-labeled nucleotides (Roche). The PCR conditions were as follows: initial denaturation at 95°C for 2 min, followed by 35 cycles at 95°C for 1 min, 58°C for 1 min and 72°C for 1 min, and then 72°C for 5 min. The two products of the PCR amplification were restricted using the NotI and SacII enzymes and gel purified on an 0.8% agarose gel using a gel extraction kit (Qiagen). The pCMV6-neo plasmid was digested using the NotI and SacII enzymes, and the 5780 bp restricted vector was gel purified in an 0.8% agarose gel using a gel extraction kit (Qiagen). The three DNA molecules were then ligated using a ligase reaction (T4 DNA ligase, Stratagene), and we thereby obtained the functionalized 6964 bp DNA. We used 1 μm-diameter, streptavidin-coated magnetic beads (Dynabeads MyOne Streptavidin C1, Dynal) at a concentration of about 7×10^6 beads per μl. About 1.4×10^7 beads (2 μl of solution) were washed three times in 1 ml of Phosphate-buffered saline (PBS); the end result was dispersed in a volume of about 10 μl. To this solution, we added 10 μl of functionalized DNA solution with a total of 10^7 molecules. After a 5-min incubation, the solution was diluted with 500 μl of 10 mM PBS at pH 8 supplemented with 0.1% Tween-20 and 3 mM NaN_3 (referred to hereafter as PBS-Tween-20).

Cell preparation

The modified DNA and magnetic beads were studied in a flow cell made of a properly functionalized capillary. For each measurement session, 250 μl of the prepared suspension (modified DNA and magnetic beads) was injected, in the absence of a magnetic field, into a glass capillary tube (1×1 mm^2 section, 5-cm long, VitroCom, Mountain Lakes, NJ) that had been functionalized as follows. First, a solution of 100 mg/ml polystyrene (average $M_W \approx 230000$, Aldrich) in toluene (purum, Riedel-de Haën) was injected into the capillary tubes. Then, the capillaries were drained and blown with compressed air. In this way, the internal walls were uniformly coated with polystyrene (46). Next, 5 μg of sheep polyclonal anti-digoxigenin antibody (Roche) was incubated in the capillary tubes for 2 h at 37°C in 100 μl with 10 mM PBS. Unbound anti-digoxigenin was eliminated by rinsing the tubes with PBS-Tween-20. The treated surface was passivated for 2 h at 37°C with a solution consisting of 10 mM PBS at pH 8 supplemented with 0.1% Tween-20, 1 mg/ml fish sperm DNA (Roche) and 3 mM NaN_3 (47). Finally, the capillary tubes were rinsed with PBS-Tween-20 and incubated for ~1h to allow the DNA to bind to the lower capillary surface. For storage, the tubes were dried with compressed air and kept at −20°C.

MTs technique

The MTs setup was assembled according to other similar apparati reported in the literature (2,48). The capillary, linked to a buffer-flow system, was placed over the objective (Nikon 100× 1.25 NA oil immersion with a 15-cm-focal-length tube lens, which leads to an actual magnification of 75×) of an inverted microscope equipped with a piezoelectric focusing system (PIFoc, Physik Instrumente). Images were acquired at a rate of 40 frames per second with a CCD camera (Marlin, Allied Vision Technologies) and were fed into a PC. From these data, we extracted the time dependence of the x, y and z positions of the magnetic bead. The magnetic field used to pull and twist the beads was generated by two cubic, 5 mm neodymium magnets with a 2-mm gap between them. A permalloy ring was placed outside the magnets to convey the magnetic field between the outer faces of the magnets. The configuration of the magnets has been previously discussed (49,50), and here we used a setup similar to that shown in Figure 2 of (49), which corresponds to the model presented in Figure 1b of (50). The magnets can be lowered (raised) to increase (decrease) the stretching force acting on the DNA. Due to the permanent magnetic moment of the bead, a rotation of the magnets around their axis induces a rotation of the bead, which induces torsion on the DNA molecules.

Data analysis

Using our MT setup, we measured three quantities: DNA extension, applied force and number of imposed turns.

DNA extension was calculated by considering the diffraction images generated at different heights of the bead (51,52). After obtaining a series of calibrating images at known positions, the actual position is obtained by comparing the acquired images to the calibrated images through a fitting algorithm.

To evaluate the force exerted on the beads by the magnetic field, we measured the mean square displacement σ^2 of the horizontal position along the x-axis (2,53) at each magnet height

$$\sigma^2 = \langle (x - \langle x \rangle)^2 \rangle \quad (1)$$

The variance in the bead excursion was evaluated considering the camera integration time and accordingly corrected (29). Then, we extracted the force F using the equipartition theorem (54)

$$F = \frac{k_B T L_e}{\sigma^2} \quad (2)$$

where k_B is the Boltzmann constant, T the temperature and L_e the DNA extension. Once the system had been calibrated, we were able to apply a known force ranging from a few fN to several pN.

Representative measurements of force F versus extension L_e obtained by the MTs technique on bare DNA are shown in Figure 1c. We concentrated our attention on the behavior of DNA at relatively low applied forces F ($F < 10$ pN), which is the so-called 'entropic' regime (2). In such a regime, the external force generated by the magnets is

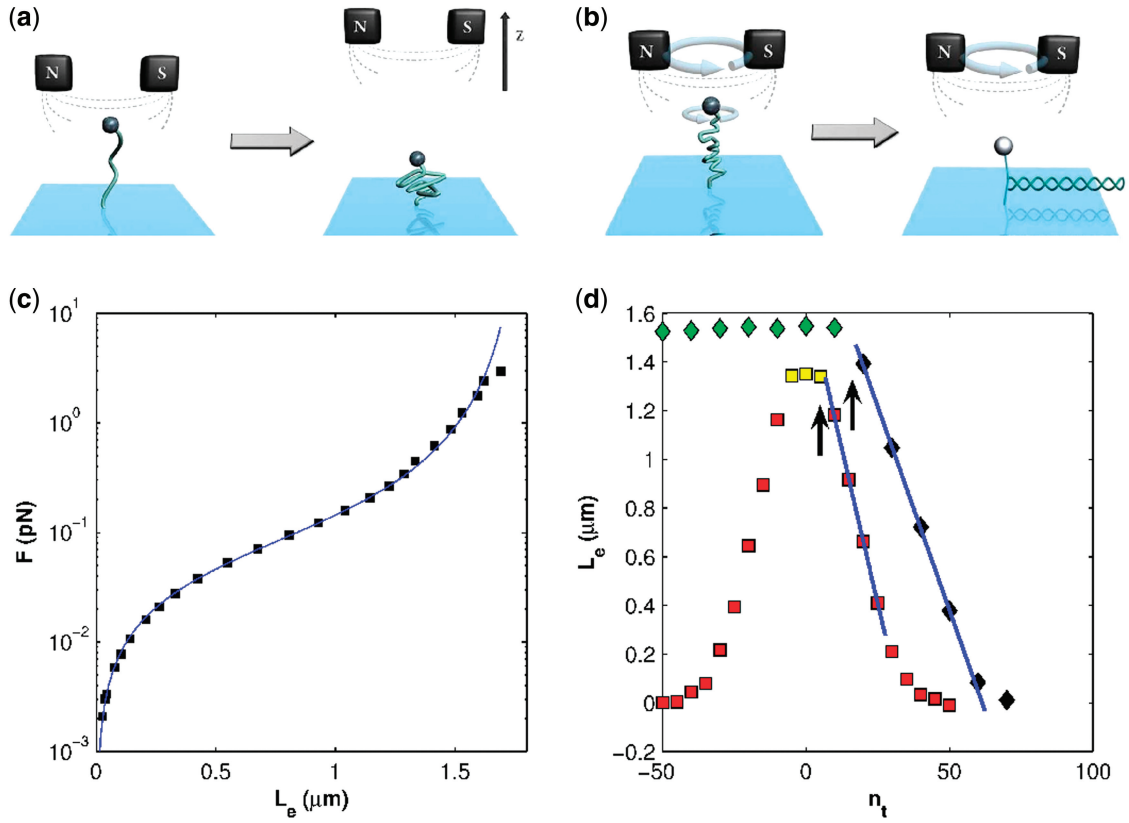

Figure 1. Schematic sketch of the MTs technique (**a**) and (**b**) and representative measurements obtained with bare DNA (**c**) and (**d**). (**C**): DNA extension L_e measured as a function of the applied force F (data taken at zero imposed turns). The continuous line represents a fit of the data with the WLC model. (a): DNA extension L_e measured as a function of the imposed turns n_t (yellow and red dots: data taken at $F = 2.96$pN; green and black dots: data taken at $F = 2.96$pN). The buckling number N_b is indicated by vertical arrows, while Δz is the slope of the linear fit (blue lines) of the descending part of the L_e versus n_t data.

counter-balanced by the decrease in entropy caused by a reduction in the number of available configurations of the DNA molecule. As shown in Figure 1c, in this regime, L_e is an increasing function of F, and the specific shape of the curve can be fitted by the worm-like chain model (WLC) (2). In this model, DNA is treated as a homogeneous, isotropic polymer with a specific value of the bending stiffness B. Accordingly, F versus L_e data are described by the following approximate interpolation formula, which considers the contour length L_o and the persistence length L_p as free parameters

$$\frac{FL_P}{k_BT} = \frac{1}{4}\left(1 - \frac{L_e}{L_0}\right)^{-2} - \frac{1}{4} + \frac{L_e}{L_0} \qquad (3)$$

Thus, $L_P = B/(k_BT)$ influences the vertical shift of the force versus extension curve, while L_o is related to the maximum asymptotic length attained by DNA at high force (29). In Figure 1a, we show a sketch describing what happens to DNA in two configurations consisting of high and low mechanical stress. As shown in Figure 1a, when the magnet is lowered, the force becomes stronger and the DNA is highly stretched by the magnetic force acting on the bead. As shown in Figure 1c, by fitting the data with Equation 3, the WLC accurately describes the data and gives values for the free parameters of $L_0 = 1.8 \pm 0.1 \mu m$ and $L_P = 45 \pm 3$nm. The value of the contour length appears to be compatible with the number of DNA base pairs when considering a sedimentation height of a few hundreds of nanometers.

By rotating the external magnets at a fixed height, the MT technique creates the possibility of applying a torque to torsionally constrained DNA. We have exploited this capability by measuring the extension L_e of a DNA molecule as a function of the number of imposed turns n_t. The obtained L_e versus n_t data are shown in Figure 1d for the representative case of bare DNA and for two different values of the applied pulling force. At low force values (yellow and red dots in Figure 1d), the L_e versus n_t data are symmetric, while at high force (see green and black dots in Figure 1d), the clockwise and anticlockwise rotations induce different behaviors due to the intrinsically chiral nature of DNA. Specifically, at low force values, we can distinguish between two different regions in the measured data: a central 'low turn' region (yellow dots in Figure 1d) where L_e is basically constant and two lateral 'high turn' regions (red dots in Figure 1d) where L_e is linearly dependent (increasing or decreasing) on n_t.

This behavior is qualitatively described by the sketch of Figure 1b. Starting from a relaxed configuration, the DNA molecule becomes more and more tangled as

the magnets rotate, and eventually plectonemes are formed. The formation of plectonemes induces a progressive linear decrease in the DNA extension, which is analogous to the decrease in extension of a twisted and tangled telephone cord.

Indeed, the topology of a torsionally constrained segment of DNA is described by two quantities: the twist number $Tw = N_{bp}/h$ (where N_{bp} is the base pair number and h the helical pitch), which corresponds to the number of helical turns in the double helix, and the writhe number W_r, which is defined as the number of times the axis of the double helix crosses itself (2). In the absence of external torque, the natural twist of DNA is Tw_0, which is obtained by considering the natural value of h ($h_0 = 10.4$ bp per turn), with $Wr_0 = 0$. Since the torsion is initially absorbed by the elastic twist deformations, the application of a torque first implies an increase in T_w while W_r remains constant. This corresponds to the 'low turn' central and symmetric region, where the DNA extension is approximately constant and does not depend on n_t (yellow dots in Figure 1d). As the torque is continuously increased, the DNA undergoes a buckling transition at a specific number of imposed turns n_b. At this point, loops or plectonemes, are formed (see Figure 1d, where n_b is indicated by the vertical arrows). Indeed, beyond the n_b number, it is energetically convenient to release energy from the elastic twisting deformations by bending the double helix, forming plectonemes, and increasing W_r instead of increasing the T_w number. Above n_b, the DNA extension decreases linearly with n_t, with a slope Δz, (see the blue fitting line in Figure 1d). Both the buckling number n_b and the slope Δz in the plectonemic region depend on the values of the applied force. Finally, by considering negative imposed turns and high force values (green dots in Figure 1d), the DNA extension is no more dependent on the rotation, because the torsion energy is mainly absorbed by denaturing (instead of writhing) the DNA and inducing the formation of denaturation 'bubbles' (2).

Furthermore, in the frame of the quoted naive model (29), the double-stranded DNA is simply represented as an elastic cylinder with a torsional constant C and a bending constant B. By minimizing the elastic energy and considering only positive values of rotations ($n_t > 0$), the model (2,48) predicts the following expressions for n_b and Δz

$$n_b = \frac{L_0}{\pi C}\sqrt{\frac{BF}{2}} \quad (4)$$

$$\Delta z = 2\pi\sqrt{\frac{B}{2F}} \quad (5)$$

According to this simplified theory, we should expect a sharp transition between the twisting region (constant DNA extension) and the plectonemic region (linearly decreasing DNA extension). In contrast, in our experiment, we observed a smooth transition between the two trends. This previously observed discrepancy is normally attributed to thermal noise or to oversimplifications in the model (2). Due to this smoothing of the curve at the transition, n_b has been extracted as the intersection value between the linear fitting of the plectonemic region and a horizontal line intercepting the maximum extension value.

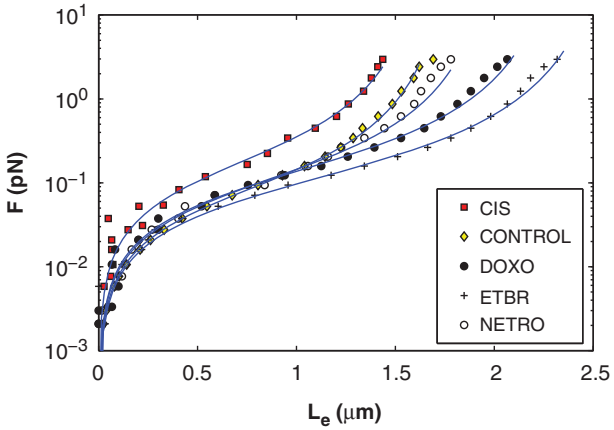

Figure 2. DNA extension L_e measured as a function of the applied force F. Data were taken at zero imposed turns for bare DNA and in presence of various drugs (see legend). The continuous lines represent fits with WLC model.

We point out that there are more rigorous mechanical models of the buckling and post-buckling behavior of chains under torsion (55–58). However, we think that the naive model is still valuable given our goal of obtaining a qualitative discrimination between different molecular interaction.

RESULTS AND DISCUSSION

Extension versus force data

To describe the mechanical modifications induced by the drugs' interaction with the DNA, we first studied the DNA extension. The results are shown in Figure 2, where we have plotted the F versus L_e data obtained with the above-described MTs technique. The measurement protocol was as follows: after binding the DNA to the bead and the capillary, we first applied an increasing force and measured the resulting extension in the absence of any drugs. This procedure gives a control measurement without drugs, which was compared to the data obtained with drugs. Next, we decreased the force by increasing the height of the magnets. Then, in the absence of applied force, we injected the drug under investigation into the capillary and measured the corresponding new DNA extension as a function of the applied force. As is apparent in the graph (Figure 2) and by considering the asymptotic length attained by the DNA at high forces, we observed that, in some cases, the extension is increased (DOXO and ETBR, length increment of ~30%), while in other cases, the extension is reduced (CIS, length decrement of ~15%). With NETRO, no relevant variations were observed. These results are easily understood by considering the molecular effects of the added drugs, and they confirm other recently published data in the literature obtained with either similar or different techniques (27,59–61). Indeed, DOXO and ETBR, two intercalators that have

comparable chemical DNA-binding behavior, induce an increase of $\Delta L = 0.34$nm for each bond (13). In contrast, the binding of CIS introduces a kink in the DNA molecules, which does not affect the contour length but reduces the maximum possible extension of the DNA (62). As a result of its mechanism of binding to DNA (minor groove binder), NETRO has no relevant effect on the extension of the nucleic acid. The results, obtained by fitting the data presented in Figure 2 with Equation. 3, are summarized in Table 1, where we have shown the measured DNA total contour length increment $\Delta L_0 = L_0$(DNA+drug)-L_0(bareDNA), the length increment due to a single bound drug molecule ΔL (as derived from the literature (13)), and the derived total number of binding events $N_F = \Delta L_0/\Delta L$.

Table 1. F versus L_e results

	ΔL_0(nm)	ΔL (nm)	N_f
ETBR	780	$\simeq$0.34	$\simeq$2300
DOXO	550	$\simeq$0.34	$\simeq$1600

ΔL_o corresponds to the total contour length increment induced by the ligands on the DNA, ΔL corresponds to the length increment induced by a single bound molecule as derived from the literature [13], and N_f is the estimated number of bound molecules

Extension versus imposed turns

To further explore the nanomechanical effects induced by drugs, we also imposed a torque on the DNA and studied the extension versus number of turns in several experimental situations. The results are shown in Figure 3, where we have illustrated the MT results obtained at low force ($F = 0.16$pN) for bare DNA and in the presence of the tested drugs. Compared to the bare DNA, the addition of drugs caused a lateral positive or negative shift (indicated in Figure 3 by the arrows labeled n_{to}) in the L_e versus n_t data. The intercalators (DOXO and ETBR) and the alkylating agent (CIS) induce a negative shift ($Tw < Tw_0$), while the minor groove binder (NETRO) induces a positive shift ($Tw > Tw_0$). In this case, the measurement protocol was slightly modified: after the control check, we injected the drug while keeping the applied force constant (i.e. without any variation in the height of the magnets). Without this procedure, it would have been impossible to measure the shift in the twisting number T_w with respect to the control value.

In the bare DNA, the number of turns $n_t = 0$ corresponds to the natural value of twist $Tw = Tw_0$, and the extension versus turn data are symmetric with respect to $n_t = 0$. The shift observed in the presence of drugs is due to a variation in the helical pitch. Indeed, the DOXO and ETBR molecules bind between two nucleobase pairs, and they relax the natural twist of a fixed angle by -23° and

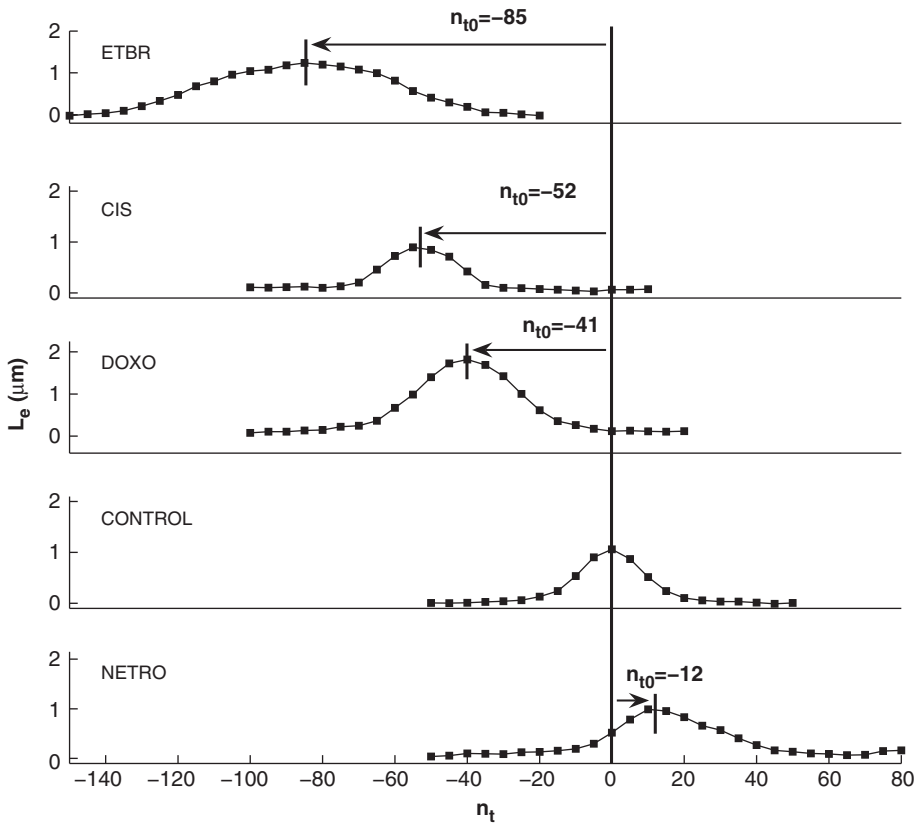

Figure 3. DNA extension L_e measured as a function of the imposed turns n_t for bare DNA and in the presence of various drugs (see legend). Data were taken at a fixed applied force $F = 0.16$pN using the protocol described in the text. n_{to} represents the shift in the twisting number T_w induced by the drugs. The continuous lines are a guide to the eye.

−27°, respectively, per molecule (13,36). In contrast, and as expected (42), NETRO overtwists the double helix by 8°. The case of CIS is different because there are three different available sites for DNA binding. Each site corresponds to a different relaxation angle and has a different probability of occupation (63,64). There is a 65% probability of CIS binding to a G–G sequence and inducing a twist of 13°, a 25% probability of binding to an A–G sequence and inducing a twist of 13°, and a 10% probability of binding to a G–X–G sequence and inducing a twist of 25°. By a simple evaluation of the statistical distribution of the number of bound CIS molecules for any possible combination of binding sites, it is possible to predict the resulting twisting number. Considering a random sequence of 5780 bp, the twisting number is expected to be between 54 and 64 turns, which is in reasonable agreement with the observed value ($n_{t0} = -52$). Table 2 shows, for each drug, the measured total twist n_{t0}, the twist angle Δn due to a single binding event as derived from the literature (36, 42, 63–66), and the derived total number $N_T = n_{t0}/\Delta n$ of bound molecules.

Effect of twist on contour length

The above-described experiments (Figure 3) were performed at a low value of applied force, where the DNA torsional behavior is symmetric. We also systematically studied the dependence of L_e versus n_t on the applied force. In Figure 4, we show two representative examples obtained in the presence of ETBR (left) and CIS (right). Considering the analogous data obtained for DNA alone (Figure 1d), we observe that the ETBR measurements (and DOXO, data not shown) present unexpected behavior. Indeed, in the twisting central region (before n_b, shown by the ellipses in Figure 4), an anomalous negative slope is present in the data for L_e versus n_t. If we extend the naive model presented in the 'Materials and Methods' section, this observation can be explained in a very simplified way by considering the double helix as a string (of backbone length L_{Helix}) wrapped around a cylindrical inner core (of radius R) (Figure 5). The linear extension L_o of the string depends, for a fixed

Table 2. L_e versus n_t results

	N_{to}	Δ_n	N_T
ETBR	−85	−27°	≃1130
CIS	−52	−13° & 25°	≃500
DOXO	−41	−11°	≃1340
NETRO	12	8°	≃540

n_{to} corresponds to the total twist induced by the ligands on the DNA, Δn corresponds to the twist angle induced by a single bound molecule as derived from the literature [36, 42, 63–66], and N_t is the estimated number of bound molecules

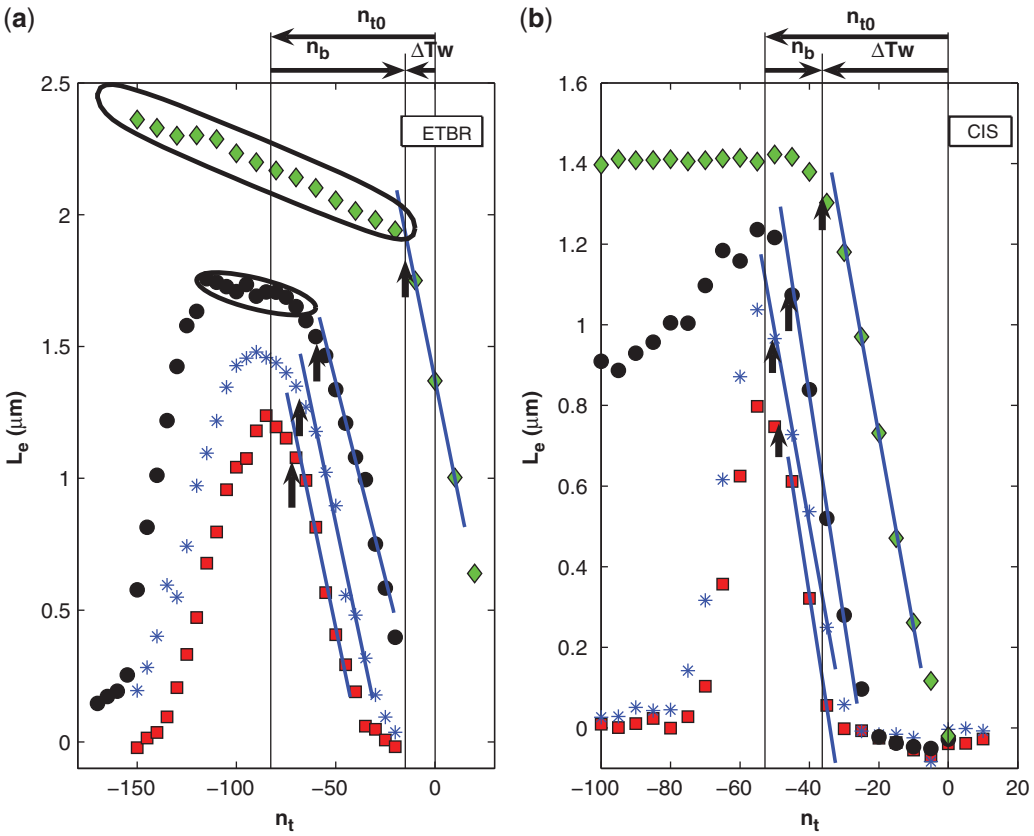

Figure 4. DNA extension L_e measured as a function of the imposed turns n_t for ETBR (**a**) and CIS (**b**) Data taken various applied force F, (squares: $F = 0.16$pN; stars: $F = 0.26$pN; circles: $F = 0.62$pN; diamonds: $F = 2.96$pN).The vertical arrows and the blue lines are the same as for Figure 1d. The ellipses in (a) empasize an anmalous slope in the data; see text for details. The horizontal double arrows indicate the values of n_b and ΔTw for the reprentive case of $F = 0.16$pN.

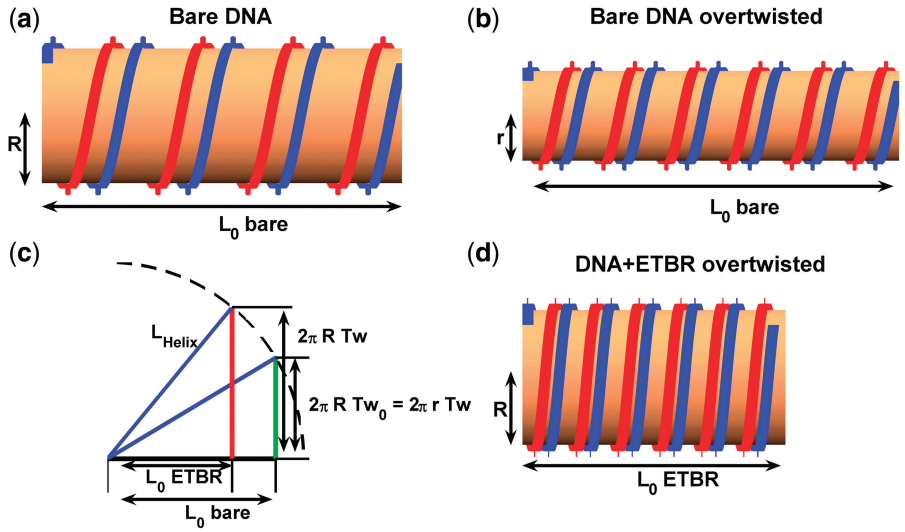

Figure 5. Schematic sketch of the naive model explaining the anomalous slope of the L_e versus n_t data observed in the presence of ETBR shown in Figure 4a. The DNA is represented by a double helix wrapped around a cylinder of radius R or r. (**a**) bare DNA of contour length L_o. Panel (**b**): over-twisted bare DNA of contour length L_o. (**c**): over-twisted DNA of reduced contour length due to the presence of ETBR. (**d**): Geometric interpretation of Equation (7). L_{Helix} is constant while L_o depends on T_w and on the radius.

radius, on the twist number as expressed by the following formula:

$$L_0 = \sqrt{L_{\mathrm{Helix}}^2 - (2\pi RTw)^2} \tag{6}$$

where the relationship between T_w and n_t is the following:

$$\begin{cases} Tw - Tw_0 \equiv \Delta Tw = n_t, & \text{if } n_t < n_{t0}+n_b \\ Tw - Tw_0 \equiv \Delta Tw = n_{t0}+n_b, & \text{if } n_t \geq n_{t0}+n_b \end{cases} \tag{7}$$

According to this extension of the naive model, in the absence of ligands, the cylinder is empty and is taken to be compressible. Then, at a low number of imposed turns, the torsion simply induces a shrinkage of the DNA core while keeping L_o, and as consequence L_e, constant (see Figure 5b). Conversely, in the presence of intercalators, the radius R can be considered constant due to the steric hindrance of the drugs. Such ligands induce a reduction of the inner core's compressibility; thus, an increase in the turn number requires a decrease in the DNA extension (see Figure 5c). The anomalous slope depends on the binding characteristics of the drug under investigation: ligands acting as intercalators increase the incompressibility of the DNA inner core, while minor groove binders and alkylating agents do not have this capability. The slope of the extension versus turn data in the central region is compatible, in our simplified model, with an inner core diameter $2R \cong 0.8$ nm (see formula (6)), which is similar to the thickness of a nucleobase pair.

Analysis of the plectonemic region

Considering now the plectonemic region (the linearly decreasing region of data in Figure 4), by exploiting the fitting method described in the Materials and Methods section, for each drug and for each applied force it is possible to obtain an evaluation of the buckling number n_b and the slope Δz. The resulting data are shown in Figure 6 for the two representative cases of ETBR and CIS as a function of the force F. The dependence of n_b as a function of F (Figure 6a) appears to be reasonably well described by a power law ($n_b \propto F^{\alpha}$) with exponent α. This power law behavior is also confirmed for all of the other investigated drugs (data not shown), and in Table 3, we have reported the corresponding values of α obtained by the fitting procedure.

Analogously, we have plotted Δz as a function of the applied force F (Figure 6), and the data appear basically constant. All of the drugs under investigation (data not shown) show a similar constant behavior or a slightly negative power law ($\Delta z \propto F^{-\beta}$) with a value of the exponent β close to zero (see Table 3).

It should be noted that the naive mechanical model predicts a specific power law dependence of n_b and Δz as a function of the applied force ($n_b \propto F^{1/2}$; $\Delta z \propto F^{-1/2}$), see Equation. (4)&(5) This prediction is not confirmed by the data, as previously reported in the literature (2,55–58). This discrepancy is not really surprising, considering the reasonable possibility that B increases with the imposed overtwist. More specifically, the n_b and Δz parameters, according to the simplified model, are obtained by minimizing the energy resulting from three combined terms: the energy required to pull the bead, the energy to bend the DNA, and the energy to twist the double helix. The buckling instability occurs when the third factor is larger than the sum of the other two. At larger forces, the value of the first two factors increases and induces an increase in n_b, as observed in all of the experiments. On the other hand, the two contributions that determine Δz are opposite, and the resulting behavior is neither trivial nor predictable by simple

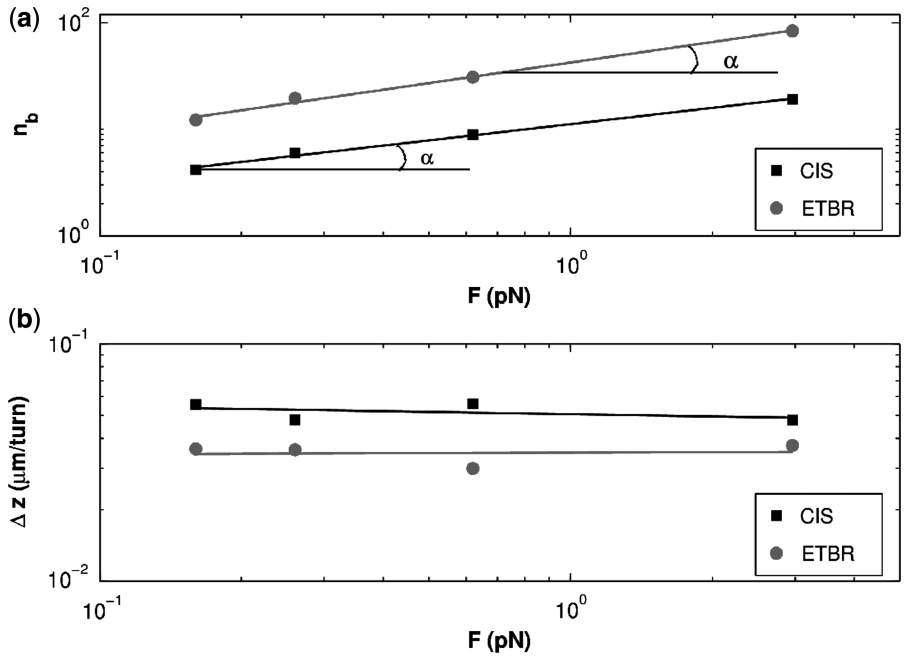

Figure 6. Buckling number n_b and plectonemic slope Δz plotted as a function of the applied force F for CIS and ETBR. Data obtained from measurements of Figure 4 with the fitting procedure described in the text (see Data Analysis section). The lines show a power law fit to the data. The corresponding fitting exponents α and β are reported in Table 3.

Table 3. Exponents α and β of the power law dependence of n_b and Δz as a function of F

	α	β
ETBR	0.6	610^{-3}
DOXO	0.8	−0.3
NETRO	0.4	110^{-2}
CIS	0.5	310^{-2}
CONTROL	0.6	−0.2
THEORY	0.5	−0.5

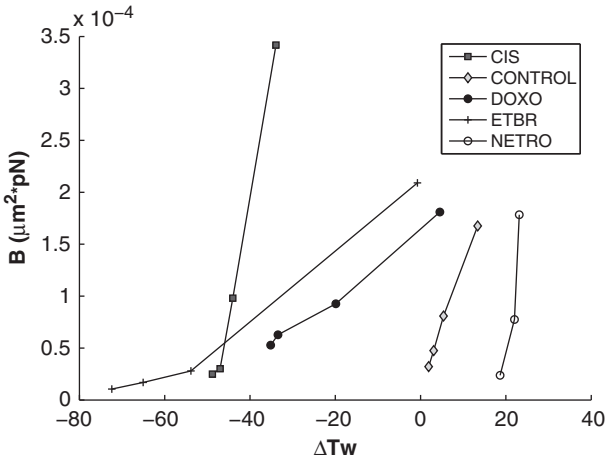

Figure 7. Bending constant B plotted as a function of the imposed overtwist $\Delta Tw = Tw\text{-}Tw_0$. Data were obtained for various drugs (see legend) and derived by using the procedure described in the text. Lines are guides to the eye.

heuristic considerations. In any case, after the buckling instability is reached, any further turns imposed on the DNA do not increase its twist number (T_w) but instead increase the number of formed plectonemes (W_r number) while keeping B and C fixed. We have assumed local validity of the naive model in the plectonemic region (for $n_t > n_b$) where the twist of the DNA is constant. Accordingly, we have considered Equation (5), and by simply solving it for B, we obtained: $B = F\Delta z^2/(2\pi^2)$. Then, from the data shown in Figure 6, we have derived a qualitative estimate of B for all of the applied forces. The obtained B values are shown in Figure 7 as functions of the absolute twist difference with respect to the bare DNA, $\Delta Tw = Tw\text{-}Tw_0$. As is apparent in Figure 7, the DNA bending characteristics depend on the imposed overtwist, and the different drugs result in different behaviors. The two intercalators (ETBR and DOXO) show a mild dependence of B on ΔT_w due to the initial DNA elongation induced by the drug. The minor groove binder and alkylating agent studied (NETRO and CIS) do not modify the stronger dependence of B on ΔT_w observed with bare DNA, but their data are shifted to the positive (NETRO) and negative (CIS) regions of the plot, i.e. for positive or negative ΔT_w. Indeed, the relevant result shown in Figure 7 is the fact that this analysis allows us to easily and qualitatively distinguish among the different families of drugs. While all of the previous data analyses are not truly able to discriminate between different interaction mechanisms of drugs, we suggest that the consideration of B versus ΔT_w allows one to make a distinction between various binding characteristics.

CONCLUSIONS

In this article, we have measured some nanomechanical properties of DNA in the presence of various binding molecules by means of MTs techniques. We have observed that the presence of drugs induces a variation in the DNA length and a shift in the extension versus turn data. In the case of intercalators, we have also observed an anomalous dependence of DNA extension on the number of imposed turns that is not due to plectonemic formation. This result has been qualitatively justified by considering the molecular interaction mechanisms involved in the binding phenomenon and by assuming a simple excluded volume model. Finally, we have observed that the DNA bending characteristics depend on the imposed turn number. Intercalators are able to modify this dependence, while minor groove binders and alkylating agents cannot. We suggest that this dependence indicates a general method for classifying different DNA-binding molecules. This discrimination can be considered as a particularly relevant result because this methodology could allow for a rapid and detailed screening of pharmaceutically active drugs. DNA is recognized as the primary target of many established antitumor agents. The efficacy of DNA-interacting agents is related to their direct effects on DNA structure or to the consequences of their binding on DNA functions. It is evident that not all DNA-interacting agents are useful as therapeutic drugs. Although the efficacy of a DNA-interacting agent is not simply related to its ability to bind DNA, its pharmacodynamic properties clearly reflect its mode of DNA-binding and its influence on DNA structure (e.g. DNA damage). Efforts focusing on rational approaches to predict optimal DNA interactions may have useful implications.

ACKNOWLEDGEMENTS

We thank F. Croccolo for valuable help in building the MT setup.

FUNDING

Funding for open access charge: University of Milano Bicocca and Fondazione IRCCS Istituto Nazionale Tumori.

Conflict of interest statement. None declared.

REFERENCES

1. Walter,N.G., Huang,C.Y., Manzo,A.J. and Sobhy,M.A. (2008) Do-it-yourself guide: how to use the modern single-molecule toolkit. *Nat. Methods*, **5**, 475–489.
2. Strick,T.R., Dessinges,M.N., Charvin,G., Dekker,N.H., Allemand,J.F., Bensimon,D. and Croquette,V. (2003) Stretching of macromolecules and proteins. *Rep. Prog. Phys.*, **66**, 1–45.
3. Neuman,K.C. and Nagy,A. (2008) Single-molecule force spectroscopy: optical tweezers, magnetic tweezers and atomic force microscopy. *Nat. Methods*, **5**, 491–505.
4. Gosse,C. and Croquette,V. (2002) Magnetic tweezers: micromanipulation and force measurements at the molecular level. *Biophys. J.*, **82**, 3314–3329.
5. Mosconi,F., Allemand,J.F., Bensimon,D. and Croquette,V. (2009) Measurement of the torque on a single stretched and twisted DNA using magnetic tweezers. *Phys. Rev. Lett.*, **102**, 078301/1–4.
6. Baumann,C.G., Smith,S.B., Bloomfield,V.A. and Bustamante,C. (1997) Ionic effects on the elasticity of single DNA molecules. *Proc. Natl Acad. Sci. USA*, **94**, 6185–6190.
7. Dholakia,K., Spalding,G. and MacDonald,M. (2002) Optical tweezers: the next generation. *Phys. World*, **15**, 31–35.
8. van Mameren,J., Modesti,M., Kanaar,R., Wyman,C., Wuite,G.J. and Peterman,E.J. (2006) Dissecting elastic heterogeneity along DNA molecules coated partly with Rad51 using concurrent fluorescence microscopy and optical tweezers. *Biophys. J.*, **91**, L78–80.
9. Curtis,J.E., Koss,B.A. and Grier,D.G. (2002) Dynamic holographic optical tweezers. *Opt. Comm.*, **207**, 169–175.
10. Noom,M.C., van den Broek,B., van Mameren,J. and Wuite,J.L.G. (2007) Visualizing single DNA-bound proteins using DNA as a scanning probe. *Nat. Methods*, **4**, 1031–1036.
11. Moffitt,J.R., Chemla,Y.R., Smith,S.B. and Bustamante,C. (2008) Recent advances in optical tweezers. *Annu. Rev. Biochem.*, **77**, 205–228.
12. Bustamante,C., Bryant,Z. and Smith,S.B. (2003) Ten years of tension: single-molecule DNA mechanics. *Nature*, **421**, 423–427.
13. Coury,J.E., McFaillsom,L., Williams,L.D. and Bottomley,L.A. (1996) A novel assay for drug-DNA binding mode, affinity, and exclusion number: scanning force microscopy. *Proc. Natl Acad. Sci. USA*, **93**, 12283–12286.
14. Dame,R.T., Wyman,C. and Goosen,N. (2000) H-NS mediated compaction of DNA visualised by atomic force microscopy. *Nucleic Acids Res.*, **28**, 3504–3510.
15. Abels,J.A., Moreno-Herrero,F., van der Heijden,T., Dekker,C. and Dekker,N.H. (2005) Single-molecule measurements of the persistence length of double-stranded RNA. *Biophys. J.*, **88**, 2737–2744.
16. Friese,M.E.J., Nieminen,T.A., Heckenberg,N.R. and Rubinsztein-Dunlop,H. (1998) Optical alignment and spinning of laser-trapped microscopic particles. *Nature*, **394**, 348–350.
17. Paterson,L., MacDonald,M.P., Arlt,J., Sibbett,W., Bryant,P.E. and Dholakia,K. (2001) Controlled rotation of optically trapped microscopic particles. *Science*, **292**, 912–914.
18. Smith,S.B., Finzi,L. and Bustamante,C. (1992) Direct mechanical measurements of the elasticity of single DNA molecules by using magnetic beads. *Science*, **258**, 1122–1126.
19. Bustamante,C., Marko,J.F., Siggia,E.D. and Smith,S. (1994) Entropic elasticity of lambda-phage DNA. *Science*, **265**, 1599–1600.
20. Smith,S.B., Cui,Y. and Bustamante,C. (1996) Overstretching B-DNA: The elastic response of individual double-stranded and single-stranded DNA molecules. *Science*, **271**, 795–799.
21. Strick,T.R., Allemand,J.F., Bensimon,D., Bensimon,A. and Croquette,V. (1996) The elasticity of a single supercoiled DNA molecule. *Science*, **271**, 1835–1837.
22. Nollmann,M., Stone,M.D., Bryant,Z., Gore,J., Crisona,N.J., Hong,S.C., Mitelheiser,S., Maxwell,A., Bustamante,C. and Cozzarelli,N.R. (2007) Multiple modes of Escherichia Coli DNA gyrase activity revealed by force and torque. *Nat. Struct. Mol. Biol.*, **14**, 264–271.
23. Koster,D.A., Croquette,V., Dekker,C., Shuman,S. and Dekker,N.H. (2005) Friction and torque govern the relaxation of DNA supercoils by eukariotic topoisomerase IB. *Nature*, **434**, 671–674.
24. Koster,D.A., Palle,K., Bot,E.S.M., Bjornsti,M.A. and Dekker,N.H. (2007) Antitumour drugs impede DNA uncoiling by topoisomerase I. *Nature*, **448**, 213–217.
25. Revyakin,A., Ebright,R.H. and Strick,T.R. (2005) Single-molecule DNA nanomanipulation: Improved resolution through use of shorter DNA fragments. *Nat. Methods*, **2**, 127–138.
26. Revyakin,A., Liu,C., Ebright,R.H. and Strick,T.R. (2006) Abortive initiation and productive initiation by RNA polymerase involve DNA scrunching. *Science*, **314**, 1139–1143.
27. Lee,N.K., Park,J.S., Johner,A., Obukhov,S., Hyon,J.Y., Lee,K.J. and Hong,S.C. (2008) Elasticity of cisplatin-bound DNA reveals the degree of cisplatin binding. *Phys. Rev. Lett.*, **101**, 248101/1–4.

28. Conroy,R. (2007) Force spectroscopy with optical and magnetic tweezers. In Noy,A. (ed.), *Handbook of Single-Molecule Biophysics*. Springer, New York, pp. 23–96.
29. Vilfan,I.D., Lipfert,J., Koster,D.A., Lemay,S.G. and Dekker,N.H. (2009) Magnetic tweezers for single-molecule experiments. In Hinterdorfer,P. and van Oijen,A. (eds), *Handbook of Single-Molecule Biophysics*. Springer, New York, pp. 371–395.
30. Haber,C. and Wirtz,D. (2000) Magnetic tweezers for DNA micromanipulation. *Rev. Sci. Instrum.*, **71**, 4561–4570.
31. Langner,K.M., Kedzierski,P., Sokalski,W.A. and Leszczynski,J. (2006) Physical nature of ethidium and proflavine interactions with nucleic acid bases in the intercalation plane. *J. Phys. Chem. B*, **110**, 9720–7.
32. Krautbauer,R., Pope,L.H., Schrader,T.E., Allen,S. and Gaub,H.E. (2002) Discriminating small molecule DNA binding modes by single molecule force spectroscoy. *FEBS Lett.*, **510**, 154–158.
33. Vladescu,I.D., McCauley,M.J., Rouzina,I. and Williams,M.C. (2005) Mapping the phase diagram of single DNA molecule force-induced melting in the presence of ethidium. *Phys. Rev. Lett.*, **95**, 158102.
34. McCauley,M., Hardwidge,P.R., Maher,L.J. III and Williams,M.C. (2005) Dual binding modes for an HMG domain from human HMGB2 on DNA. *Biophys. J.*, **89**, 353–364.
35. Ros,A., Hellmich,W., Duong,T. and Anselmetti,D. (2004) Towards single molecule analysis in PDMS microdevices: from the detection of ultra low dye concentrations to single DNA molecule studies. *J. Biotechnol*, **112**, 65–72.
36. Hayashi,M. and Harada,Y. (2007) Direct observation of the reversible unwinding of a single DNA molecule caused by the intercalation of ethidium bromide. *Nucleic Acids Res.*, **35**, e125/1–7.
37. Wang,J.C. (1974) The degree of unwinding of the DNA helix by ethidium: I. titration of twisted PM2 DNA molecules in alkaline cesium chloride density gradients. *J. Mol. Biol.*, **89**, 783–801.
38. Minotti,G., Menna,P., Salvatorelli,E., Cairo,G. and Gianni,L. (2004) Anthracyclines: molecular advances and pharmacologic developments in antitumor activity and cardiotoxicity. *Pharmacol. Rev.*, **56**, 185–229.
39. Zlatanova,J., Yaneva,J. and Leuba,S.H. (1998) Proteins that specifically recognize cisplatin-damaged DNA: a clue to anticancer activity of cisplatin. *FASEB J.*, **12**, 791–799.
40. Kelland,L. (2007) The resurgence of platinum-based cancer chemotherapy. *Nat. Rev. Cancer*, **7**, 573–584.
41. Kopka,M.L., Yoon,C., Goodsell,D., Pjura,P. and Dickerson,R.E. (1985) The molecular origin of DNA-drug specificity in netropsin and distamycin. *Proc. Natl Acad. Sci. USA*, **82**, 1376–1380.
42. Triebel,H., Bär,H., Walter,A., Burckhardt,G. and Zimmer,C. (1994) Modulation of DNA supercoiling by interaction with netropsin and other minor groove binders. *J. Biomol. Struct. Dyn.*, **11**, 1085–1105.
43. Malcolm,A.D. and Snounou,G. (1983) Netropsin increases the linking number of DNA. *Cold Spring Harb. Symp. Quant. Biol*, **47**, 323–326.
44. Snounou,G. and Malcolm,A.D.B. (1983) Production of positively supercoiled DNA by netropsin. *J. Mol. Biol.*, **167**, 211–216.
45. Triebel,H., Bar,H., Geuther,R. and Burckhardt,G. (1995) Netropsin-induced changes of DNA supercoiling; sedimentation studies. In *Progress in and Colloid Polymer Science*. Springer, Berlin, pp. 45–54.
46. Allemand,J.F., Bensimon,D., Jullien,L., Bensimon,A. and Croquette,V. (1997) pH-dependent specific binding and combing of DNA. *Biophys. J.*, **73**, 2064–2070.
47. Strick,T.R., Allemand,J.F., Bensimon,D. and Croquette,V. (1998) Behavior of supercoiled DNA. *Biophys. J.*, **74**, 2016–2028.
48. Strick,T., Allemand,J.F., Croquette,V. and Bensimon,D. (2000) Twisting and stretching single DNA molecules. *Prog. Biophys. Mol. Biol.*, **74**, 115–140.
49. Lipfert,J., Haoand,X. and Dekker,N.H. (2009) Quantitative modeling and optimization of magnetic tweezers. *Biophys. J.*, **96**, 5040–5049.
50. Brogioli,D. *Design of magnetic tweezers for DNA manipulation*. http://arxiv.org/abs/0907.4601 (25 June 2010, date last accessed).
51. Strick,T.R., Allemand,J.F., Bensimon,D., Bensimon,A. and Croquette,V. (2003) Apparatus and method for the manipulation and testing of molecules, and in particular of DNA. Pub.No, US 2003/0027187 A1: [0052],[0053],[0054], [0052],[0053],[0054].
52. Strick,T.R., Allemand,J.F., Bensimon,D., Bensimon,A. and Croquette,V. (2003) Apparatus and method for the manipulation and testing of molecules, and in particular of DNA. Pub.No, US 2003/0166262 A1: [0052],[0053],[0054], [0052],[0053],[0054].
53. Te Velthuis,A.J.W., Kerssemakers,J.W.J., Lipfert,J. and Dekker,N.H. (2010) Quantitative guidelines for force calibration through spectral analysis of magnetic tweezers data. *Biophys. J.* (in press).
54. Gittes,F. and Schmidt,C.F. (1998) Signals and noise in micromechanical measurements, in: Laser tweezers in cell biology. In Sheetz,M.P. (ed.), *Methods in Cell Biol*. Academic Press, San Diego, CA, pp. 129–156.
55. Zachmann,D.W. (1979) Nonlinear analysis of twisted axially loaded elastic rod. *Q. Appl. Math.*, **37**, 67–72.
56. Neukirch,S. (2004) Extracting DNA twist rigidity from experimental supercoiling data. *Phys. Rev. Lett.*, **93**, 198107/1–4.
57. Goyal,S., Perkins,N.C. and Lee,C.L. (2005) Nonlinear dynamics and loop formation in Kirchhoff rods with implications to the mechanics of DNA and cables. *J. Comp. Phys.*, **209**, 371–389.
58. Purohit,P.K. (2008) Plectoneme formation in twisted fluctuating rods. *J. Mech. Phys. Solids*, **56**, 1715–1729.
59. Tessmer,I., Baumann,C.G., Skinner,G.M., Molloy,J.E., Hoggett,J.G., Tendler,S.J.B. and Allen,S. (2003) Mode of drug binding to DNA determined by optical tweezers force spectroscopy. *J. Mod. Opt.*, **50**, 1627–1636.
60. Rocha,M.S., Ferreira,M.C. and Mesquita,O.N. (2007) Transition on the entropic elasticity of DNA induced by intercalating molecules. *J. Chem. Phys.*, **127**, 105108/1–7.
61. Lee,N.K., Park,J.S., Johner,A., Obukhov,S., Hyon,J.Y., Lee,K.J. and Hong,S.C. (2009) Investigation of the elasticity of a cisplatin-DNA adduct via single-molecule measurements and bimodal modeling. *Phys. Rev. E*, **79**, 041921/1–8.
62. Hou,X.M., Zhang,X.H., Wei,K.J., Ji,C., Dou,S.X., Wang,M., Li,W.C. and Wang,P.Y. (2009) Cisplatin induces loop structures and condensation of single DNA molecules. *Nucleic Acids Res.*, **37**, 1400–1410.
63. Bellon,S.F., Coleman,J.H. and Lippard,S.J. (1991) DNA unwinding produced by site-specific intrastrand cross-links of the antitumor drug cis-diamminedichloroplatinum(II). *Biochemistry*, **30**, 8026–8035.
64. Jamieson,E.R. and Lippard,S.J. (1999) Structure, recognition, and processing of cisplatin-DNA adducts. *Chem. Rev.*, **99**, 2467–2498.
65. Zeman,S.M., Depew,K.M., Danishefsky,S.J. and Crothers,D.M. (1998) Simultaneous determination of helical unwinding angles and intrinsic association constants in ligand-DNA complexes: The interaction between DNA and calichearubicin B. *Proc. Natl Acad. Sci. USA*, **95**, 4327–4332.
66. Mukherjee,A., Lavery,R., Bagchi,B. and Hynes,J.T. (2008) On the molecular mechanism of drug intercalation into DNA: a simulation study of the intercalation pathway, free energy, and DNA structural changes. *J. Am. Chem. Soc.*, **130**, 9747–9755.